TRI-PP-79-18
Jun 1979

The variation of pionic X-ray intensity with atomic number[1]

R.M. Pearce, G.A. Beer, M.S. Dixit, S.K. Kim,
J.A. Macdonald, G.R. Mason, A. Olin
University of Victoria and TRIUMF, Victoria, B.C., Canada V8W 2Y2

C. Sabev
CERN, Exp. Phys., Geneva 4, CH-1211, Switzerland

W.C. Sperry
Central Washington University, Ellensburg, WA, U.S.A. 98926

C. Wiegand
Lawrence Berkeley Laboratory, Berkeley, CA, U.S.A. 94720

Abstract

Pionic X-ray intensities have been measured for 57 elemental targets. For each transition, in addition to the broad maximum as a function of Z expected from the Auger effect and the strong absorption, local intensity maxima are observed near Z values of closed atomic shells.

(submitted to Canadian Journal of Physics)

[1]Work supported in part by Natural Sciences and Engineering Research Council of Canada.

Introduction

The intensities of X rays from exotic atoms (μ^-, π^-, K^-) have been observed to vary with the atomic number of the stopping target. A comprehensive survey [1] of kaonic X ray intensities has shown intensity variations with Z of a factor of four. Some pionic X ray intensity variations were also reported by Kunselman [2].

At present, there is no comprehensive theory to explain the details of these intensity variations. However, some general features of the intensity curves as a function of Z can be understood qualitatively [3] in terms of the Auger effect reducing the intensities of transitions at low Z and nuclear absorption of the strongly interacting particles reducing the X ray yield at high Z.

The present paper reports results of an extensive survey of the relative pionic X ray intensities for 57 elemental targets from lithium to uranium. Because of the availability of relatively higher pion beam intensities, it has been possible to study the more interesting low yield transitions with $|\Delta n| > 1$ in addition to making more precise measurements of the $|\Delta n| = 1$ transitions.

Experimental procedure

The experiment was performed on the low momentum meson channel M9 at TRIUMF. The 100 MeV/c 2×10^5 π^- beam was degraded in polyethylene, so that approximately one-half stopped in the target. Pion stops were identified by a $1 \cdot 2 \cdot 3 \cdot \bar{4}$ coincidence in a four-

scintillator telescope. The contaminant electrons and muons in the beam ($\sim 10^5$ s^{-1}) were suppressed by their range difference with respect to the pions. The position of the pion beam in the bending plane of the channel was monitored by two additional scintillators mounted on either side of the degrader. This helped ensure that the transverse distribution of pion stops in the target was kept constant.

The targets were in the form of disks 8.9 cm in diameter and typically 2 g/cm^2 thick. Some had thin mylar windows, depending on the physical and chemical properties of the particular element. The target disks were mounted, eight at a time, in a remote-controlled rotatable wheel. In each group of eight, one target was carried over from the previous group for consistency checks. The target wheel was mounted at 58° to the beam axis.

X rays were detected in an ultra pure germanium detector 3 cm in diameter by 1 cm thick, and mounted perpendicular to and 13.6 cm from the beam axis viewing the target from the back. The singles rate in the Ge detector in this geometry was $\sim 10^4$ s^{-1}. The Ge timing signal was derived from a constant fraction discriminator fed by a timing filter amplifier. The fast coincidence resolving time with the stop signal was 50 ns. Data were recorded in 1000 s runs in a Nuclear Data 2400 pulse height analyzer. The overall electronic efficiency, determined by a stop-rate dependent pulser gated into the spectrum with the data, was typically 70%. The

efficiency of the detector itself was measured using a ^{133}Ba source of known specific activity located at the center of the target position. The energy calibration was determined from ^{133}Ba, ^{75}Se and ^{241}Am sources for beam-on conditions. The detector resolution was about 900 eV FWHM at 250 keV.

The more than 350 X ray peaks were fitted using least squares techniques to Gaussian line shapes and a linear background. In the majority of cases, the width of the Gaussian and the parameters of the background were free in the fitting procedure. However in the two 5-4 cases ^{73}Ta and ^{67}Ho with the large quadrupole splitting [4,5], the intensities were obtained by summing the counts in excess of a linear background.

Self-absorption corrections

X rays originating within the target are attenuated mainly by photoelectric processes at low energies. At higher energies, incoherent scattering contributes. The photoelectric cross section was obtained from the data of ref. 6 by three-point Lagrangian interpolation on the reduced variable $E^{3/2}\,\sigma_{photo}$. The incoherent cross section was obtained by linear interpolation.

The self-absorption calculations were complicated because the distribution of pion stops, and therefore of X ray sources along the beam axis, had a Gaussian shape with FWHM = 1.3 ± 0.3 g/cm^2 in CH_2, which is of the same order as the typical target thickness of

2 g/cm^2. If the pion stopping distribution has the form $\exp(-\gamma^2x^2)$ where x is the distance in g/cm^2 measured along the target detector axis, x = b (a negative number) is the upstream face of the particular target, and x = a is the downstream face of the target which is the side where the X ray detector is located, then in a one-dimensional approximation the probability of the X ray escaping in the direction of the detector is

$$S = \int_b^a \exp(-\gamma^2x^2) \cdot \exp(-\mu[a-x])\, dx \Big/ \int_b^a \exp(-\gamma^2x^2)dx$$

$$= \exp(-\mu a+[\mu/2\gamma]^2) \cdot \frac{\mathrm{erf}(\gamma a-\sigma/2\gamma) - \mathrm{erf}(\gamma b-\sigma/2\gamma)}{\mathrm{erf}(\gamma a) - \mathrm{erf}(\gamma b)},$$

where $\mu = \mu_{photo} + \mu_{incoh}$.

The accuracy of this one-dimensional treatment was checked at a limited number of μ values by three-dimensional computer simulations of the target-detector geometry. The agreement with S was found to be within 5% even at the highest absorption values of 3 cm^2/g. From the three-dimensional calculations the effective solid angle was found to be 0.035 sr.

Allowances were made for the Z dependence of the distribution of π stops in each target when calculating S in two ways:

i) the depth in the target of the center of the stopping distribution was made equal to the range in the particular target of the 12.2 MeV pions emerging from the degrader; and

ii) the spatial width of the stopping distribution was made proportional to the range of 12.2 MeV pions in the particular target.

The pion beam intensity was adjusted occasionally by repositioning the slits at the dispersed focus at the mid plane of the pion channel. The possibility of this affecting the momentum spread of the pions, and therefore S, was investigated by repeated runs at different slit settings but no significant effect was observed.

Errors

The various errors in X ray intensity per pion stop are discussed in this section, with particular attention being paid to errors which might be systematic in Z. The errors in the case $|\Delta n| = 1$ are summarized in Table 1 under the headings "relative" and "normalization".

1. Relative errors are those which would cause a scatter of intensity values about their correct value in the absence of normalization errors. Only relative errors are shown in the figures. The relative errors include statistical uncertainties due to the finite number of counts; these were in the range 1 to 3% for $|\Delta n| = 1$, and 5 to 25% for $|\Delta n| = 2$ and 3. Errors due to target positioning were estimated from repeated runs to be approximately 2%. Errors from dead time corrections were

less than 2%. Fluctuations in the position of the pion spot on the target are estimated to have introduced negligible uncertainties. There is only one source of *relative* error in the calculation of the escape probability S: this arises because the assumed stopping distribution is not known exactly and the target thicknesses are not identical. When $S \simeq 0.8$ and $\mu \simeq 0.1$ cm^2/g for the high Z cases in the 4-3 and 5-4 transitions, for example, this relative error is approximately 1%. However when $S \simeq 0.1$ and $\mu \simeq 2.5$ g/cm^2, say at Z = 20 in the 5-4 transition, the relative error can amount to 20%. No data are reported for lines with $\mu > 3$ g/cm^2.

The relative errors discussed above are not expected to simulate the periodic intensity variations observed.

The total relative error for $|\Delta n| = 1$ transitions from the above considerations, from the scatter of points from smooth behavior, and from the reproducibility of repeated points, is $\sim$5% for $S \simeq 0.8$ and of the order of 20% for $S \simeq 0.1$. For the $|\Delta n| = 2$ and 3 transitions, the relative errors are dominated by statistical uncertainties.

2. The normalization errors arising from factors which are constant for all transitions appear next in Table 1. These factors include uncertainty in determining the total number of pion stops (15%). However this error is not expected to vary with Z. The germanium counter absolute efficiency was

uncertain by 15%, but the relative efficiency variation with energy was well known.

Finally in Table 1 there are normalization errors from effects which are expected to change smoothly and monotonically with energy. When $\mu \simeq 0.1$ cm^2/g, the absolute error of 6% [6] in the cross section causes errors of only 2% in the escape probability S. However when $\mu \simeq 2.5$ cm^2/g, the corresponding error in S is approximately 8%. The uncertainty of the spatial stopping distribution also causes normalization errors in S in the case of targets of equal thickness. For $\mu = 0.1$ cm^2/g, the normalization error is $\sim$5%, while for $\mu = 2.5$ cm^2/g, the error may be as large as $\sim$30%.

In the case of those X rays which were broadened by the strong interaction, a semi-empirical factor was applied to the intensities to correct the procedure of fitting a Gaussian to what was actually a convoluted Lorentz-Gaussian shape. This introduced an estimated error of 5% in the worst cases. Again this systematic error is essentially monotonic in Z.

To summarize, the total normalization error may amount to 25% but the uncertain factors are either constant or vary monotonically in Z and thus are not expected to introduce the observed intensity variations. Since the emphasis in the present work was on the relative intensities, we have normalized our intensities to an average of the published absolute measure-

ments (see next section). This has been done for all transitions with a single factor 0.70 which is compatible with our estimated normalization error of ∿25%.

Results

The figures show our normalized X ray intensities per pion stop with their relative errors discussed in the previous section, but for other data [2,7] show absolute values and errors. Pruy's work [7] in particular was concerned with obtaining absolute values. Figs. 1 and 2 show the 3-2, 4-2 and 5-2 transitions. In these transitions the pion wave function overlaps the nucleus and the X ray intensities are consequently increasingly depleted by nuclear absorption, particularly towards larger Z values. At low Z, competition from the Auger effect is responsible for the lowered X ray intensities in these transitions. The curves are predictions from a standard computer code which modelled the following processes in the atomic cascade of the pion: electric dipole radiation, pion decay, nuclear absorption [8], and $\Delta\ell = \pm 1$ K and L Auger processes, assuming that 2 K electrons are always present. In this model the initial atomic states were assumed to occur only at $n = 17$ with a distribution in angular momentum of $(2\ell+1)\exp(-a\ell)$. The solid line corresponds to $a = 0$, the short dashes to $a = 0.1$, and the long dashes to $a = 0.2$. Our 7.1 ± 0.3% value at $Z = 5$ is the average of separate runs 6.1 ± 0.5, 7.8 ± 0.5, and 7.3 ± 0.5%.

There are no previous data for comparison with the 4-2 and 5-2 intensities shown in Fig. 2.

Figs. 3 through 6 show $|\Delta n| = 1$ transitions where nuclear absorption and Auger processes are less dominant, and more striking intensity variations, presumably of atomic origin, are seen to occur. In the 4-3 and 5-4 transitions the dependence agrees well with previous work [2]. The errors in the higher transitions 6-5 and 7-6 become progressively larger because of increasingly large self-absorption corrections.

Figs. 7 through 10 show the $|\Delta n| = 2$ transitions, which are less intense than the $|\Delta n| = 1$ transitions, since the latter include the transitions between highly populated "circular orbits" $\ell = n-1$. The $|\Delta n| = 2$ transitions (apart from 5-3 transition) show intensity variations larger than $|\Delta n| = 1$, a result which is expected since the cascade through a particular circular orbit tends to sum the intensities over the complete range of previous ℓ values [9]. Only isolated intensity values have been reported previously [2] for $|\Delta n| = 2$, and these are shown on the figures.

The low intensity 8-6 transitions were not completely resolved from the high intensity 6-5 transitions at low Z; e.g., the energy separation in units of the instrumental full width at half maximum was 1.40, 1.79 and 2.70 at Z = 50, 60 and 70, respectively. A pair of these overlapping, or close to overlapping, peaks was fitted simultaneously with a common value of the instru-

mental width which was left free in the fitting procedure. However, there remains the possibility of a systematic error in the intensities of the weaker 8-6 transition, particularly in the region of low Z.

The abrupt increase in the 8-6 predictions in Fig. 10 (and also in the 8-5 predictions of Fig. 13) as Z decreases through 71 is caused by the feeding transitions, Auger K 9-8, suddenly becoming energetically possible. Although the energy available for the 9-8 transition varies as Z^2, the K shell binding energy does not strictly vary as Z^2 because of electron shielding and as a result the two energy curves as a function of Z intercept. The intercept occurs at approximately Z = 71 and 63.4 keV, but is sensitive to the value assumed for the K shell binding energy. We have assumed that the presence of the n = 9 pion reduces the nuclear charge by one and have taken the Z-1 binding energies from reference 6. Unfortunately, the experimental data are not sufficiently accurate or complete to verify this predicted discontinuity.

Figs. 11 through 13 show the measured $|\Delta n| = 3$ intensities together with the isolated measurements reported by others [7]. The $|\Delta n| = 3$ intensities are lower, and the variations are larger, than the $|\Delta n| = 1$ intensities, as expected from arguments similar to those in the $|\Delta n| = 2$ case above. The statistical uncertainties are relatively large because of the low intensities.

The intensity variations for pionic atoms are, in general, smaller than the kaonic variations shown in Fig. 14. This may be due to the following reasons: (i) the kaon cascade starts at higher n values (e.g. for maximum overlap with the 1s electron $n_K = 31$ and $n_\pi = 17$); (ii) the nuclear absorption of the kaon during the cascade is larger than the pion (e.g. for p state capture in the case of helium $\Gamma_K = 4\times10^{15}/n^3\ s^{-1}$ and $\Gamma_\pi = 5\times10^{12}/n^3\ s^{-1}$) [10].

The asymmetry in the pionic variations makes the location of the intensity peaks inexact but it appears that the maximum 5-4 yield occurs at Z = 39 whereas for the 4-3 transition the maximum occurs at Z = 34. In order for this to be possible it is necessary that there be other transitions feeding the n=4 level with maxima at Z < 39. Our data seems to be consistent with this requirement: the only measured transitions are at 7-4 (3%) and 6-4 (8%), and have maxima at 34.

Conclusions

The general trend of the experimental intensity variations as a function of Z in Figs. 1 to 13 is to some extent reproduced by the predictions of the cascade model. (These intensity predictions do not include an arbitrary normalization constant.) The decreased intensity at high Z and low n is caused by the relatively large overlap of the meson wave function with the nucleus and the consequent absorption of the meson. The decreased X ray intensity at low Z and large n is caused directly by competition from the Auger

effect (e.g. for Z = 6, Auger probabilities are larger than radiative rates for n>4 [3]). The Auger process also depletes the low Z X ray intensity in an indirect manner: Auger transitions are favored at low Z and tend to produce lower angular momentum states than do radiative transitions. This is because radiative transitions prefer $\Delta\ell = -1$ with large $|\Delta n|$, while Auger transitions prefer $\Delta\ell = -1$ with a minimum $|\Delta n|$ consistent with energy considerations [3]. Thus Auger processes at low Z indirectly cause more mesons to be lost during the cascade.

In addition to the broad maxima caused by the strong interaction and the Auger effect, there are sharper peaks whose origin may lie in a combination of the strong interaction and some atomic effects. Since the dominant initial atomic capture process is an Auger process, the electronic configuration of the host material Z may affect the probability $P(Z,n,\ell)$ of a meson being captured into an atomic state with quantum numbers n, ℓ, and affect the nuclear absorption probability.

It is not meaningful to fit the observed peaks by various Z dependent initial distributions in the cascade model because of the large number of free variables. In fact, the assumptions made in the predictions that all captures occur at n = 17 with a distribution $(2\ell+1)\exp(-a\ell)$ have no firm basis and are more in the nature of a convenient parameterization [11] which is in general use.

We have attempted to evaluate the pion data and the kaon data [1] shown in Fig. 14 following the observation [1,12] that the intensity peaks tend to occur near elements with closed electron shells. The Z = 36 shell has the best correlation with well defined maxima in the cases π 4-3, π 6-4, π 7-5, π 7-4, π 8-5, K 6-5, K 7-6, and with less definite maxima in π 5-4, π 5-3 and K 8-7. The Z = 50 shell shows well defined maxima in π 8-6, K 7-6, K 8-7, K 9-8, and lesser maxima in π 6-5 and perhaps in π 4-3, π 5-4, π 6-4 and K 10-9. The Z = 18 shell has badly defined maxima in π 5-3, π 6-3 and K 6-5, and perhaps at π 4-3, K 5-4 and K 7-6. The Z = 18 shell is also approximately correlated with a minimum in the muon K_β/K_α intensity ratio [13]. The Z = 85 shell has poorly determined maxima in the K 8-7, K 9-8 and K 10-9. There is also a suggestion of a maximum in a few cases at the end of the lanthanide rare earth sequence at Z = 72.

Although theoretical studies of the initial distribution have been attempted [14], there is no comprehensive theory incorporating electronic shell effects. It might be expected that the interpretation would be simpler for elements than for chemical compounds where the electronic configurations of the valence electrons may be altered according to the nature of the chemical bond. There is also the possibility of the formation of "large mesic molecules" where the initial mesonic orbits are comparable to the size of the molecules of the target [15].

Given that the peaks appear to have the periodicity of the atomic table, it is not clear which of the many periodic atomic properties are affecting the initial distribution. One candidate which has been proposed [16] is the electron density in the outer part of the atom. Another possibility is the bond length or lattice spacing. It has been proposed [17] that short bond lengths may limit the angular momentum allowed at time of initial capture and that nuclear capture in low ℓ states during the subsequent cascade then depletes the X rays in the lower lying states. Although there appears to be some correlation with bond length, the unusually large bond lengths [18] of 5.63 atomic units for cesium, 5.22 for rubidium, 4.96 for potassium, and 4.66 for barium do not correspond to unusually large X ray intensities as would be expected in this model.

The differential energy loss at low meson velocities is another atomic property which is cyclic in Z. It has variations of a factor of almost four with maxima at approximate Z's of 18, 35, 55 [19]. This effect, which was not considered in the bond length arguments summarized above, appears to act in the wrong direction to explain the observed variations: regions of high slowing-down power would be expected to correspond to regions of low capture velocity and therefore of low angular momentum and of low X ray intensity.

Although the observed intensities appear in general to be continuous functions of Z, there is the prediction of Auger discontinuities as in Figs. 10 and 13 and two observed discontinuities: there is a well corroborated effect in $\pi\ ^3He$ and $\pi\ ^4He$ in which the intensity ratio 2-1/3-1 averaged over several experiments and the two isotopes is 1.09 ± 0.05 in the liquid phase [20,21,22] and 0.39 ± 0.03 in the gas phase [23]. There is also some evidence [24] that the muonic X ray intensity ratio 5-3/4-3 for amorphous selenium divided by the same ratio for metallic selenium is 0.74 ± 0.06.

The probability of a K shell Auger process is directly proportional to the number of K electrons present. The predictions shown in the curves in the figures were made with the assumption that two K electrons are always present. The isolated predictions at low Z shown as triangles assume that a K shell vacancy from a previous Auger event was not refilled. A comparison with the experimental intensities, particularly the 5-4, 6-4, 7-4 and 7-5, indicates that refilling of the K shell is usually complete. An exception to this rule is pure helium, where the electron cannot be returned for energy reasons.

REFERENCES

1. C.E. Wiegand and G.L. Godfrey, Phys. Rev. A, 9, 2282 (1974); G.L. Godfrey and C.E. Wiegand, Phys. Lett. B, 56, 255 (1975)
2. A.R. Kunselman, Lawrence Berkeley Lab. Rep. UCRL-18654 (1969)
3. Y. Eisenberg and D. Kessler, Phys. Rev. 123, 1472 (1961); Y. Eisenberg and D. Kessler, Phys. Rev. 130, 2352 (1963)
4. R.A. Carrigan *et al.*, Phys. Lett. B, 25, 193 (1967)
5. P. Ebersold *et al.*, Nucl. Phys. A, 296, 493 (1978)
6. E. Storm and H.I. Israel, Nuclear Data Tables A, 7, 565 (1970)
7. H.S. Pruys, Swiss Institute for Nuclear Research Rep. RR-78-007, July 1978
8. C. Sayre and A. Olin, University of Victoria Rep. VPN-77-8 (1977)
9. W. Sperry, G.A. Beer, M.S. Dixit, J.A. Macdonald, G.R. Mason, A. Olin, R.M. Pearce, C. Sabev and C. Wiegand, submitted to Phys. Lett. B
10. J.G. Fetkovich and E.G. Pewitt, Phys. Rev. Lett. 11, 290 (1963)
11. D. Kessler *et al.*, Phys. Rev. Lett. 18, 1179 (1967)
12. A. Backenstoss, *Atomic Physics 4*, edited by G. zu Putlitz, E.W. Weber and A. Winnacker (Plenum, New York, 1975) 163
13. D. Quitmann, R. Engfer, U. Hegel, P. Brix, G. Backenstoss, K. Goebel and B. Stadler, Nucl. Phys. 51, 609 (1964)
14. M. Leon and R. Seki, Nucl. Phys. A, 282, 445 (1977); M. Leon and J.H. Miller, Nucl. Phys. A, 282, 461 (1977)

15. L.I. Ponomarev, Ann. Rev. Nucl. Sci. 23, 395 (1973); S.S. Gershstein and L.I. Ponomarev, *Muon Physics* (Academic Press, New York, 1973)
16. R. Kunselman *et al.*, Phys. Rev. Lett. 36, 446 (1976)
17. G.T. Condo, Phys. Rev. Lett. 33, 126 (1974)
18. D.O. Welch and K.G. Lynn, Phys. Stat. Sol. (b), 77 277 (1976)
19. T.K. Alexander *et al.*, Phys. Lett. B, 74, 183 (1978); B.M. Latta and P.J. Scanlon, Phys. Rev. A, 13, 1370 (1976)
20. G.R. Mason, G.A. Beer, D.A. Bryman, M.S. Dixit, S.K. Kim, J.A. Macdonald, A. Olin, R.M. Pearce, M. Krell and J.S. Vincent, Phys. Lett. B, 74, 179 (1978); and submitted to Phys. Lett. B
21. G. Backenstoss *et al.*, Nucl. Phys. A, 232, 519 (1974)
22. B.O. Sapp, Ph.D. Thesis, The College of William and Mary, Virginia, U.S.A. (1974)
23. R. Abela *et al.*, Nucl. Phys. A, 232, 519 (1974)
24. L. Tauscher *et al.*, Phys. Lett. B, 27, 581 (1963)

Table 1. Sources of error in % for the intensity per pion stop of $|\Delta n| = 1$ X rays in the case of target absorption $\mu = 0.1$ cm^2/g. Values for $\mu = 2.5$ cm^2/g in brackets.

1. Relative Errors	
Statistics	1 - 3%
Target position	2
Dead time correction	2
Beam position	< 2
Change of slit setting	< 2
Target thickness	1 (20)
Total relative error	5% (20)
2. Normalization Errors	
a. Constant	
Stop signal	15
Counter efficiency	15
Solid angle	3
b. Monotonic in E	
σ_{photo} and σ_{incoh}	2 (8)
Stop distribution	5 (30)
(Broad lines only	5)
Total normalization error	∿ 25% (31)

Figure captions

Fig. 1 The percentage yield of n = 3 to n = 2 pionic X rays per pion stop as a function of atomic number for elemental materials. • shows the present work and the relative errors (see text), × shows Kunselman [2], and □ Pruys [7]. The curves are predictions from a standard cascade calculation with atomic capture only at n = 17 with a distribution in the ℓ states varying as $(2\ell+1)\exp(-a\ell)$. The solid curve is a = 0, short dashes a = 0.1, long dashes a = 0.2. Δ shows predictions with no K shell refilling.

Fig. 2 The π 4-2 and 5-2 transitions. See caption Fig. 1.

Fig. 3 The π 4-3 transition. See caption Fig. 1.

Fig. 4 The π 5-4 transition. See caption Fig. 1.

Fig. 5 The π 6-5 transition. See caption Fig. 1.

Fig. 6 The π 7-6 transition. See caption Fig. 1.

Fig. 7 The π 5-3 transition. See caption Fig. 1.

Fig. 8 The π 6-4 transition. See caption Fig. 1.

Fig. 9 The π 7-5 transition. See caption Fig. 1.

Fig. 10 The π 8-6 transition. See caption Fig. 1.

Fig. 11 The π 6-3 transition. See caption Fig. 1.

Fig. 12 The π 7-4 transition. See caption Fig. 1.

Fig. 13 The π 8-5 transition. See caption Fig. 1.

Fig. 14 The percentage yields of kaonic X rays per kaon stop [1].

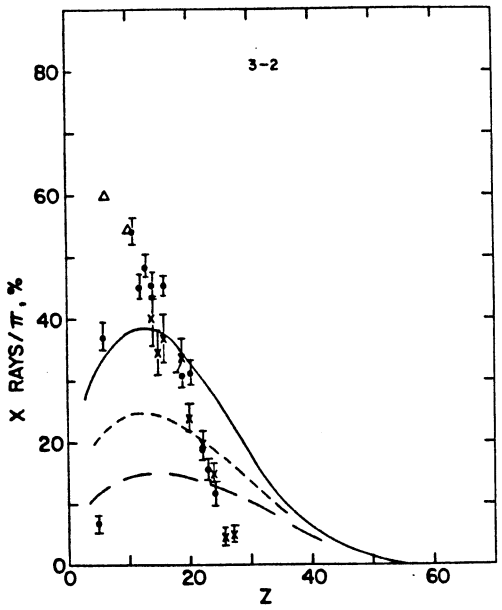

Fig. 1

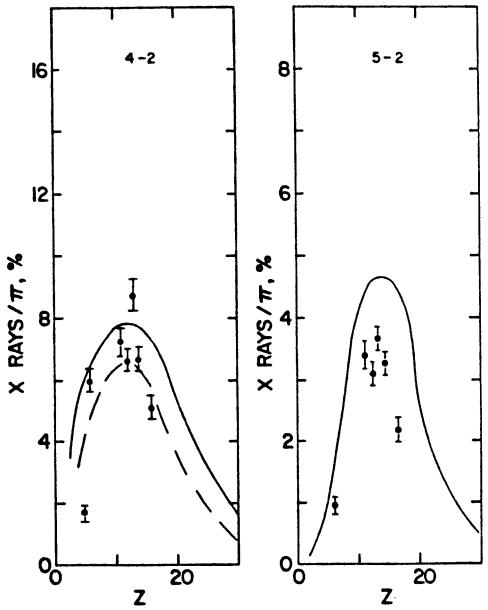

Fig. 2

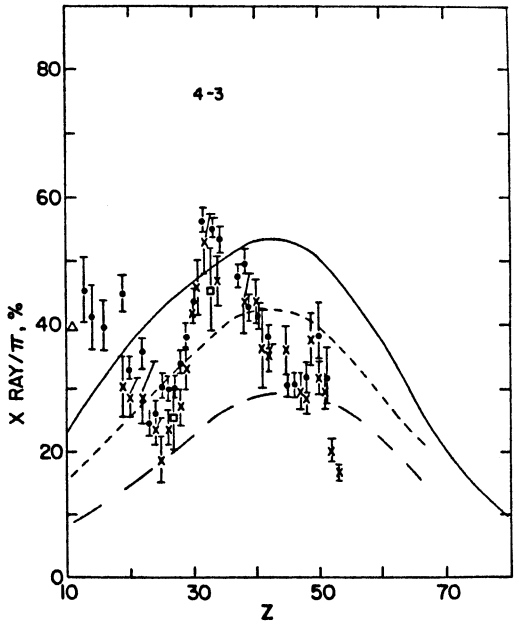

Fig. 3

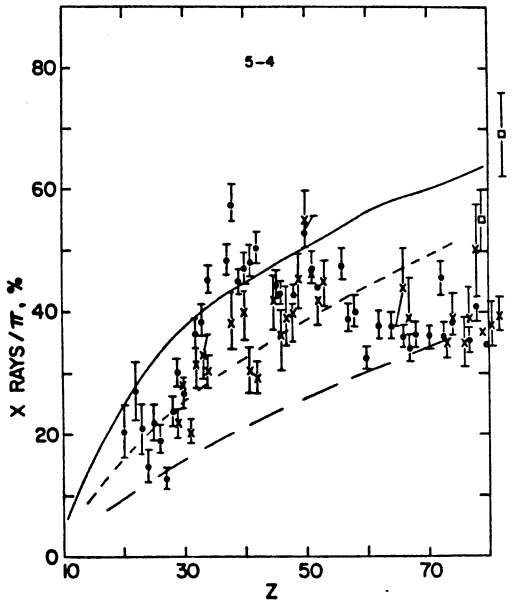

Fig. 4

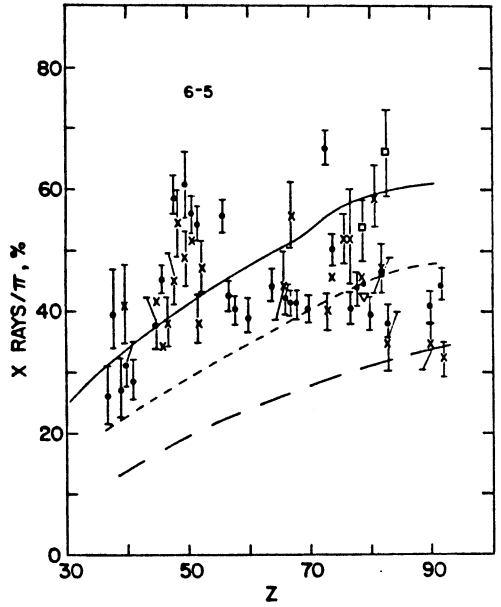

Fig. 5

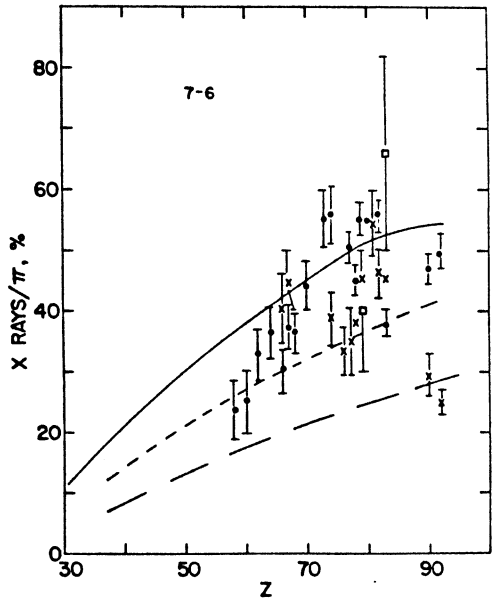

Fig. 6

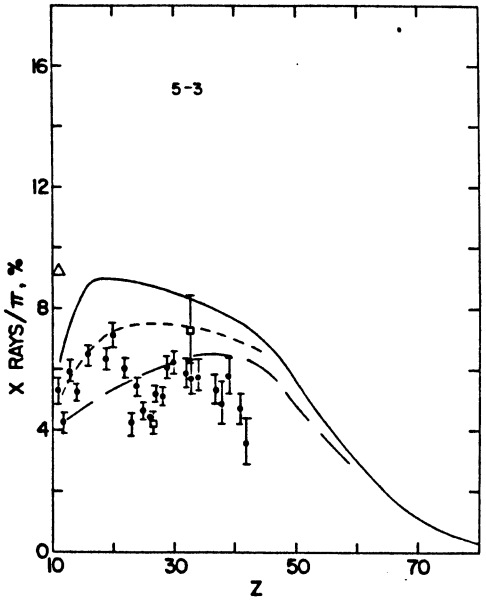

Fig. 7

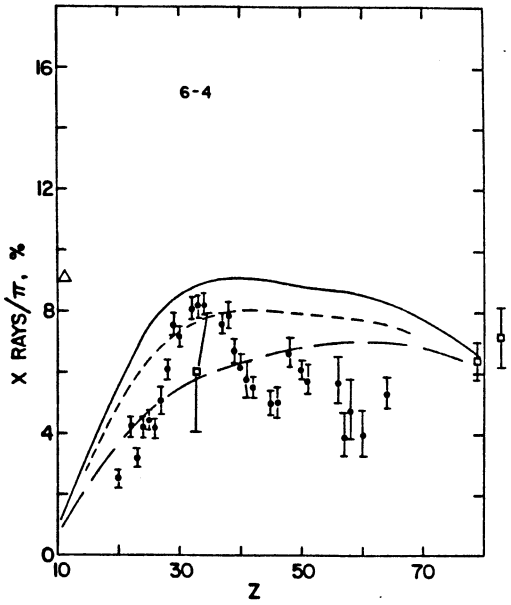

Fig. 8

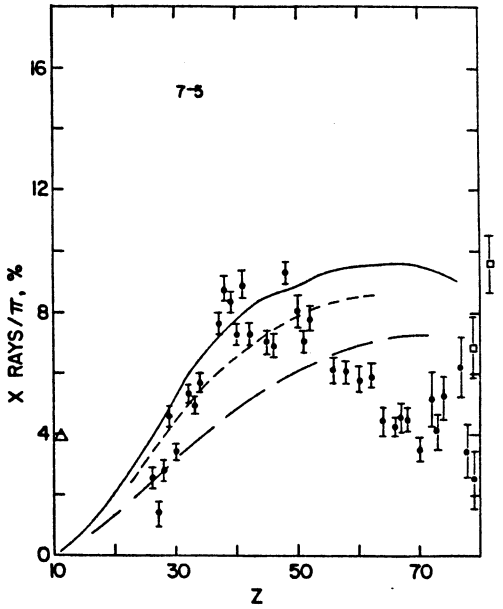

Fig. 9

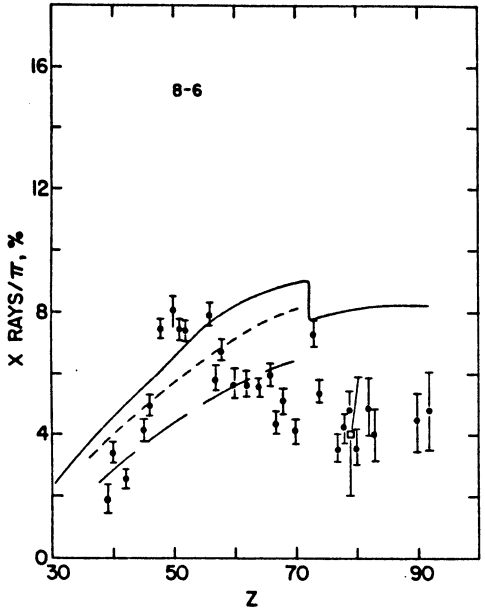

Fig. 10

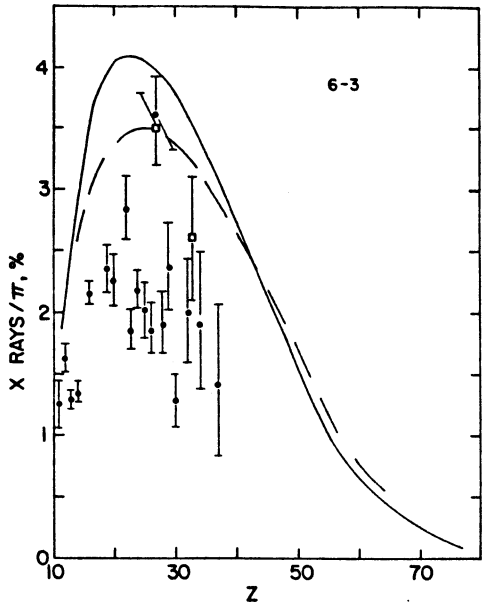

Fig. 11

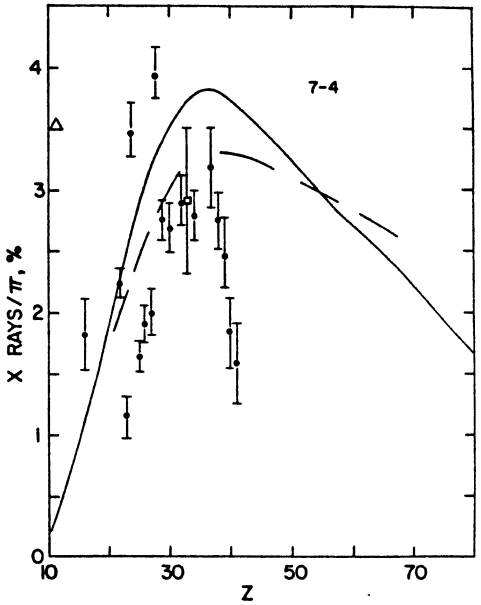

Fig. 12

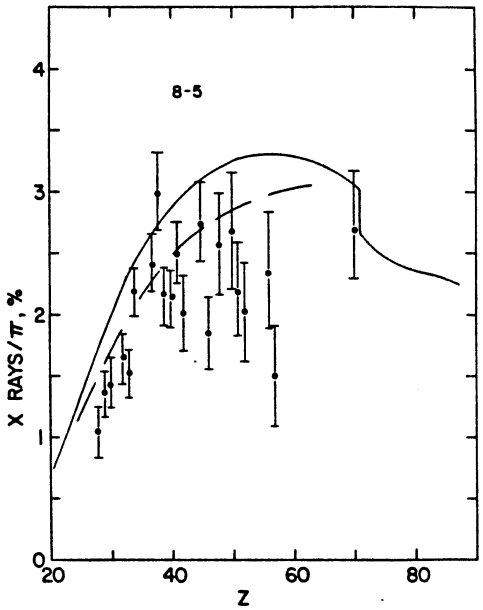
8-5
X RAYS/π, %
Z
0
1
2
3
4
20
40
60
80

Fig. 13

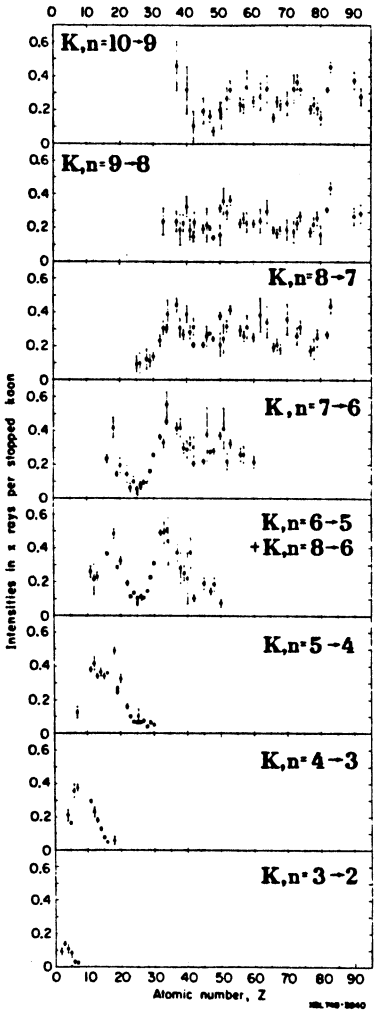
K,n=10→9
K,n=9→8
K,n=8→7
K,n=7→6
K,n=6→5
+K,n=8→6
K,n=5→4
K,n=4→3
K,n=3→2
Intensities in x rays per stopped kaon
Atomic number, Z
0 10 20 30 40 50 60 70 80 90
0 0.2 0.4 0.6

Fig. 14